EPJ Web of Conferences **302**, 09005 (2024) https://doi.org/10.1051/epjconf/202430209005
SNA + MC 2024

Branchless Collisions for Reducing Spatial Correlations in Continuous Energy Monte Carlo Power Iteration

T. Bonnet[1,*] and *H.* Belanger[2,**]

[1]Engineering Department, University of Cambridge, Trumpington St., Cambridge CB2 1PZ, UK
[2]Department of Mechanical, Aerospace, and Nuclear Engineering, Rensselaer Polytechnic Institute, 110 8th St., Troy, NY, USA

Abstract. Branchless collisions are customarily used in time-dependent Monte Carlo simulations and have been recently introduced in Monte Carlo power iteration. Previous works have shown that branchless collisions are very efficient in quenching spatial correlations in a multi-group framework, and a preliminary work was previously conducted in order to extend the use of branchless collisions to continuous energy. In that work, two variants of branchless collisions were introduced: branchless on the material, and branchless on the isotope. In this work, we analyse in depth the effect of using branchless collisions in realistic systems on spatial correlations, and we show that performing branchless collisions on the material consistently results in a smaller effect of spatial correlations than when using a standard branching collision algorithm.

1 Introduction

The Monte Carlo method is customarily used in reactor physics whenever reference solutions are required, typically using the k-eigenvalue power iteration method [1]. A set number of neutrons are first sampled from an arbitrary source distribution and undergo a sequence of free flights and collisions where the particle may undergo scattering, capture or fission. Upon capture or fission, a neutron life (or history) is terminated, and the termination of the last history in a set of neutrons marks the end of a *generation*. Neutrons produced by fission are kept in a separate bank and serve as the source for starting the subsequent generation. After a finite number of generations the distribution of fission neutrons converges to the fundamental eigenstate. This fundamental eigenstate can be estimated by averaging over different realizations of the fission source at equilibrium [1].

Depending on how fission particles are sampled, correlations between neutrons arise in the fission source. Collisions are generally processed in a manner which does not reflect the physical process, and the Monte Carlo game is kept unbiased by assigning statistical weights to neutrons. Usually, the fission source is filled using a branching algorithm; upon collision or fission, a given number of fission neutrons are sent to the fission source, meaning that multiple neutrons in the fission source at the beginning of a generation typically originate from the same common ancestor in the previous generation. Over successive generations,

*e-mail: tlfab2@cam.ac.uk
**e-mail: belanh2@rpi.edu

an increasing number of neutrons will share a common ancestor in one of the previous generations, and will thus be correlated. For historical reasons (and to reduce the computation time), averaging is generally performed over successive generations (once the fission source has converged to the fundamental eigenmode) and the statistical error is estimated by assuming that the samples thus obtained are identically and independently distributed. We shall call this average *ergodic*, and similarly the sample variance of scores obtained this way shall be referred to as the *ergodic* (*apparent*) variance. We also define the *ensemble* average over truly statistically independent samples, and we call the sample variance of such scores the *ensemble* (*true*) variance. In general, positive correlations between fission neutrons lead to an underestimation of the true variance by the apparent variance, especially in systems with a large dominance ratio [2]. Nonetheless the true variance can be asymptotically recovered for a large number of active generations, number which depends on the dominance ratio of the system [3].

In addition to this well known phenomenon, it has been recently shown that fission-induced correlations can lead to patchy neutron spatial distributions, also known as neutron clustering [4]. While neutron clustering has no effect on the estimated average of quantities of interest such as fluxes or reaction rates, it may lead to strongly non-Poisson fluctuations in the spatial distribution of neutrons, and these may also affect the reliability of the statistical errors on such space-dependent observables. Introducing a wide range of estimators, previous work has shown that in the context of multi-group Monte Carlo calculations, using branchless collision algorithms could considerably lower the effect of spatial correlations [5, 6]. Different implementations of branchless collisions in the case of continuous energy were tested in Ref. [7] and their respective effect on spatial correlations was investigated in the case of a simple homogeneous box using Shannon entropy and the neutron genealogy. It proved hard to discriminate between the different methods using only these space-independent observables.

The goal of this work is to extend this analysis to more sophisticated benchmark problems in continuous energy, using diagnostic tools more adapted to the analysis of spatial correlations such as introduced in Ref. [5]. First, in Section 2, we shall recall the definition of the Feynman moment and the Shannon entropy as well as their interpretation for correlation diagnostics. The details of the Monte Carlo algorithms for sampling collisions are discussed in Section 3. Numerical results and comments will be provided in Section 4 for a homogeneous reflected box and the 3D C5G7 benchmark. Finally, we provide concluding remarks in Section 5.

2 Observables of interest

The effect of correlations on the fission source can be given a physical interpretation: positively correlated particles tend to cluster together, which is clearly apparent in the distribution of fission source particles. As such, the fission source is often used to characterize the effect of correlations on power iteration calculations.

2.1 Shannon entropy

An estimate of the strength of neutron correlations can be given by the Shannon entropy of the weighted fission source positions defined by

$$S(g) = -\sum_{i=1}^{B} p_i(g) \log_2(p_i(g)), \tag{1}$$

where $p_i(g)$ is the probability that a neutron falls within the i'th space bin at generation g. As positive correlations lead to self-organization, the Shannon entropy decreases with increasing correlations. Therefore, if the Shannon entropy of the fission source in a simulation deviates from the ideal entropy (i.e. the entropy corresponding to neutrons independently distributed following the fundamental eigenstate), then there is a high degree of clustering in the simulation. The use of the Shannon entropy for correlation diagnostics is however afflicted by two limitations: the ideal entropy is generally unknown; and all spatial information is lost due to space-averaging. In practice, we would like to have an observable that is (i) space-dependent, and (ii) has a known ideal value in the absence of correlations.

2.2 Feynman moment

To address our desire to have a space-dependent quantity with a known ideal value, we introduce a new local observable: the Feynman moment of tally O in space-bin i, which is defined as

$$Y_{O_i} = \frac{\mathbf{V}[O_i]}{\mathbf{E}[O_i]}, \tag{2}$$

where $\mathbf{V}[O_i]$ denotes the true variance of O_i and $\mathbf{E}[O_i]$ denotes its average value. We stress that $\mathbf{V}[O_i]$ is the variance of the estimator and not the variance of the mean of the estimator. When performing power iteration calculations, one generally obtains the apparent variance instead of the true variance, however, in this work, we will assume that the number of active generations is large enough that the apparent variance has converged to the true variance[1].

As explained in Ref. [5], the value of the Feynman moment can be given a physical interpretation: if $Y_O = 1$, the fluctuations undergone by O are Poisson-like; when this value is different from unity, fluctuations within the bin differ significantly from those of a Poisson distribution, and correlations potentially affect the behaviour of the variance of the tally. Note that as long as correlations exist, the value of the Feynman moment depends on the bin size. A value of unity for a given bin size means that the effect of correlations for this particular bin size is negligible, which may not be the case for a different bin size. Additionally, if instead of unit weight particles we consider particles of weight α, it is easy to show that if these particles of weight α are Poisson distributed in space, then the value of the Feynman moment of their spatial distribution is α. Hence the value of the Feynman moment can also be interpreted as the typical weight of a cluster of correlated particles for a given bin size. Therefore, the Feynman moment informs us of the presence of spatial correlations within the neutron population.

We shall apply the Feynman moment and the Shannon entropy to the fission source tally. They will be denoted simply by S (entropy) and Y_i (Feynman moment of the fission source in bin i). For the sake of conciseness, we will restrict ourselves to energy integrated tallies.

3 Simulation methods

In the course of the simulation, neutrons undergo successive free flights interrupted by collisions. Flights and collisions are generally processed in a non-analog way, i.e. the sampling does not follow the physical laws, but the Monte Carlo game is kept unbiased by adequately assigning particles with a statistical weight. In this work, we focus on the effect of collision biasing, and we use the analog flight kernel with standard surface tracking.

[1]This assumption was verified by either taking independent replicas or examining the behavior of the apparent variance when adding more active generations.

3.1 Branching collisions

In our baseline method, collisions are processed using a 'branching' algorithm taking the following form: first, isotope i is sampled for the collision with the probability

$$P_i(\mathbf{r}, E) = \frac{N_i(\mathbf{r})\sigma_{i,t}(E)}{\Sigma_t(\mathbf{r}, E)}, \tag{3}$$

where $\sigma_{i,t}(E)$ is the total microscopic cross-section for isotope i at incident energy E, $\Sigma_t(\mathbf{r}, E)$ the total macroscopic cross-section for the material at incident energy E and position $\mathbf{r}$, and $N_i(\mathbf{r})$ is the concentration of isotope i at position $\mathbf{r}$. Implicit fission site generation is applied, and at each collision site a random number of fission neutrons are produced, given by

$$n_f = \left\lfloor \frac{w}{k_{\text{eff}}^{g-1}} \cdot \frac{\nu_{i,f}(E)\sigma_{i,f}(E)}{\sigma_{i,t}(E)} + \xi \right\rfloor, \tag{4}$$

where w is the statistical weight of the incident neutron and k_{eff}^{g-1} is the estimate of k_{eff} from the previous generation; $\nu_{f,i}(E)$ is the fission yield, and $\sigma_{i,f}$ is the microscopic fission cross-section, taken for isotope i and incident energy E. The fission neutrons have a unit weight. Several fission neutrons typically originate from the same neutron history, thus we call these branching collisions.

Capture is accounted for by implicit capture, i.e. a neutron is not killed upon absorption but has its statistical weight multiplied by the survival probability at every collision:

$$w' = w\frac{\sigma_{i,s}(\mathbf{r}, E)}{\sigma_{i,t}(\mathbf{r}, E)},$$

where $\sigma_{i,s}(E)$ is the microscopic scattering cross-section. Hence, to ensure the simulation can end, Russian roulette is applied, in our case with threshold $w_R = 0.4$ and unit survival weight. These choices are somewhat arbitrary and corresponded to an approximate optimum in terms of variance reduction and computation time for the simulation of the homogeneous system presented below. The fission bank is populated only by unit weight particles, and its size is kept close to the initial population size.

The statistical weight w_i of neutron i in the fission source at the end of a generation is adjusted using

$$w_i' = w_i\frac{N}{W}, \tag{5}$$

where N is the initial population size and W is the total statistical weight of the fission source, which ensures that every generation starts with the same total weight.

3.2 Branchless collisions

We shall compare the baseline branching collision method with two different variants of branchless collisions in continuous energy: branchless collisions on the isotope and on the material, as discussed in Ref. [7].

3.2.1 Branchless on the isotope

The branchless on isotope method requires minimal modifications to pre-existing codes. In this method, the isotope is first sampled using Eq. (3), and the reaction channel is thereafter selected according to the probabilities

$$P_{s|i} = \frac{\sigma_{i,s}(E)}{\nu_{i,f}(E)\sigma_{i,f}(E) + \sigma_{i,s}(E)} \quad \text{and} \quad P_{f|i} = \frac{\nu_{i,f}(E)\sigma_{i,f}(E)}{\nu_{i,f}(E)\sigma_{i,f}(E) + \sigma_{i,s}(E)}, \tag{6}$$

where $P_{s|i}$ and $P_{f|i}$ are the probabilities for scatter and fission respectively, having sampled the isotope i for the collision. In case scattering is sampled, the exact scattering channel ((n,n), (n,n'), $(n,2n)$, etc.) is selected in the usual manner. Regardless of whether scattering or fission was sampled, after the reaction has been processed, the new statistical weight is given by

$$w' = w\frac{\nu_{i,f}(E)\sigma_{i,f}(E) + \sigma_{i,s}(E)}{\sigma_{i,t}(E)}. \tag{7}$$

If fission is selected, then a single fission neutron is sent to the fission source, with the incident neutron's statistical weight. With this algorithm, for each neutron in the source bank there is at most one neutron sent to the fission bank, hence it is "branchless". While the weight multiplier is independent of the reaction channel, it does depend on the sampled isotope, which can lead to large fluctuations in particle weights. In order to reduce the dispersion of statistical weights, splitting is applied whenever the particle weight crosses the threshold $w_S = 2$, and Russian roulette is applied as described in Section 3.1. Additionally, if a scattering channel with a non-unit scattering multiplicity was sampled, such as $(n,3n)$, the weight of the outgoing particle must also be multiplied by the scattering yield.

3.2.2 Branchless on the material

The branchless on material method differs from the previous by first sampling the reaction channel using macroscopic cross-sections, and then sampling the isotope, given the sampled reaction [7]. In this case, the probabilities for scattering and fission are

$$P_s = \frac{\Sigma_s(\mathbf{r},E)}{\nu_f(\mathbf{r},E)\Sigma_f(\mathbf{r},E) + \Sigma_s(\mathbf{r},E)} \quad \text{and} \quad P_f = \frac{\nu_f(\mathbf{r},E)\Sigma_f(\mathbf{r},E)}{\nu_f(\mathbf{r},E)\Sigma_f(\mathbf{r},E) + \Sigma_s(\mathbf{r},E)}, \tag{8}$$

respectively. Depending on whether fission or scattering was sampled, the probability of sampling isotope i is either

$$P_{i|f} = \frac{N_i(\mathbf{r})\nu_{i,f}(E)\sigma_{i,f}(E)}{\nu_f(\mathbf{r},E)\Sigma_f(\mathbf{r},E)} \text{ or } P_{i|s} = \frac{N_i(\mathbf{r})\sigma_{i,s}(E)}{\Sigma_s(\mathbf{r},E)}. \tag{9}$$

After the reaction is sampled, the eventual outgoing neutron is assigned a new statistical weight using Eq. (7), with the macroscopic cross-sections replacing the microscopic cross-sections.

When using either branchless collision method in an exactly critical system with leakage, the total weight of the population will decrease, which is accounted for by adjusting the weight of neutrons in the fission source using Eq. 5. Weight combing is applied to the resulting population, ensuring that all fission neutrons start the next generation with unit weight, and keeping the number of source neutrons entering each generation constant [8].

4 Numerical results

In this section, we present the result of our analysis of correlations using branchless collisions (on the material or on the isotope) combined with weight combing, and using regular branching collisions. We revisit the homogeneous and reflected critical box, and we analyze the performance of each method using the Shannon entropy and the Feynman moment of the fission source, and its behaviour as a function of the bin size. Similarly, we investigate the behaviour of these methods in a 3D mini-core calculation based on the C5G7 benchmark [9]. All results presented in this paper use the JEFF-3.3 nuclear data library.

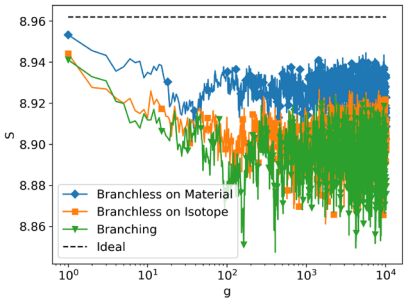

Figure 1: Shannon entropy for $B = 8^3$ up to $G = 10^4$ generations.

Isotope	Concentration [b^{-1} cm^{-1}]
$^{1}\mathbf{H}$	6.6856×10^{-2}
$^{16}\mathbf{O}$	$8.215\,787\,01 \times 10^{-2}$
$^{17}\mathbf{O}$	$3.129\,604 \times 10^{-5}$
$^{18}\mathbf{O}$	$1.688\,339 \times 10^{-4}$
$^{235}\mathbf{U}$	$2.672\,280\,41 \times 10^{-4}$
$^{238}\mathbf{U}$	$2.419\,777\,2 \times 10^{-2}$

Table 1: Isotopic compositions for the reflected homogeneous box

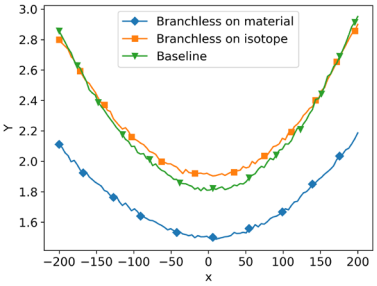

(a) Feynman moment for $\delta x = 1$ cm.

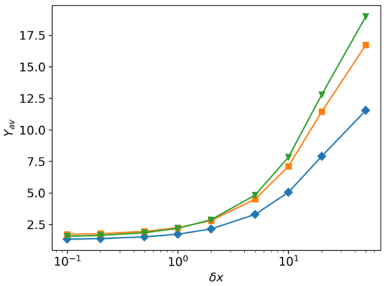

(b) Space averaged Feynman moment.

Figure 2: Feynman moments for the homogeneous box, scored over 10^5 active generations and $N = 10^4$ neutrons.

4.1 Analysis of the homogeneous reflected box calculation

We first investigate the behaviour of the homogeneous reflected box introduced in Belanger et al. Using the isotopic compositions given in Table 1 (with the thermal scattering law for light water) yields a nearly critical reflected box of half-side $L = 50$ cm. Note that the box is taken smaller than in Belanger et al. to ease the convergence of local observables. Despite the smaller size, the box is still expected to have a large dominance ratio. The calculation started from an uniform distribution in space with fixed energy $E = 1$ eV, with 200 inactive generations.

The Shannon entropy is plotted in Fig. 1. For the homogeneous box, the ideal Shannon entropy for N individuals distributed identically and independently in B boxes is known analytically (see [10]), and is represented by the dashed line. All methods share similar entropy values, but applying branchless collisions on the material appears to lead to an entropy which is closer to the ideal value, and has smaller fluctuations. This implies that branchless collisions on material lead to fewer correlations. Nonetheless, is it tricky to give the differences in the entropy of the different methods a proper intuitive interpretation.

Typical Feynman moments for the fission source integrated in y and z are shown in Fig. 2a for all three algorithms, as a function of the x position. The Feynman moment for the branchless on material method is considerably smaller than for the other two methods, indicating that correlations are mitigated by using branchless collisions on the material. The shape

shared by all Feynman moments is related to the use of reflected boundary conditions, that are known to increase correlations near the boundaries [11]. As stated above, the value of the Feynman moment can be given an intuitive interpretation, and indicates that the size of a cluster of correlated particles when using branching collisions is typically one and a half times larger than when using branchless collisions on the material. Note that for this particular bin size, using branchless collisions on the isotope essentially leads to the same amount of correlations as when using branching collisions. It is interesting to note that while the different methods had only a marginal effect on the value of the entropy, they can significantly change the value of the Feynman moment. This can be related to the fact that the effect of correlations on global tallies is almost negligible, even for systems with a large dominance ratio, while it is significant for local tallies [12].

The effect of fission-induced correlations is expected to be amplified by increasing tally bin sizes [5]. While it would be arduous to represent the position dependence of the Feynman moment as a function of the bin size $\delta x = 2L/B$, the dependency on δx of the space-averaged Feynman moment defined by

$$Y_{\text{av}} = \frac{1}{B'} \sum_{i=1}^{B'} Y_i, \tag{10}$$

already provides for interesting results, with B' being the number of bins containing fissile material. The average Feynman moment is shown in Fig. 2b as a function of the bin size. It is clear that the advantage of using branchless collisions on the material increases significantly with increasing bin sizes. This suggests that the statistical behaviour of the fission source is dominated by long-range spatial correlations. It appears that for very small values of δx, using branching collisions leads to smaller Feynman moments than when using branchless collisions on the isotope, as it was already noted in a previous work in a multi-group framework [5].

4.2 Analysis of C5G7 3D mini-core calculation

Using symmetry, the mini-core can be modelled by four assemblies representing 1/8th of the core. Reflection boundary conditions are applied on the $-x$, $-y$, and $-z$ sides, while leakage boundary conditions are applied on the opposite sides. The calculation is started again from an uniform distribution in space (provided there is fissile material), with fixed energy $E = 1$ eV, and 400 inactive generations.

The entropy is plotted in Fig. 3a. Using branchless collisions on the material once again yields higher values of the entropy, implying a lower tendency of spatial clustering. The value of the entropy for branching collisions is close, but slightly larger than that of branchless collisions on the isotope. As C5G7 is a benchmark problem for a small LWR (and we are only simulating 1/8th of the core), the dominance ratio is not expected to be as large as one would have for a full PWR. Nonetheless, this behaviour seems to suggests that performing branchless collisions on the isotope actually leads to more spatial correlations in heterogeneous systems. This question should be further investigated, especially given the fact that most time-dependent Monte Carlo code use branchless collisions on the isotope by default [13].

The Feynman moment of the fission source integrated over z when using branchless collisions on the material is plotted in Fig. 5a. The values of the Feynman moment appears to be slightly larger in the MOX assemblies than in the UO2 assemblies, and decreases quickly near leakage boundary conditions. Overall, the Feynman moment is weakly varying over the core, and the largest variations occur at assembly boundaries. Figs 5b and 5c show the

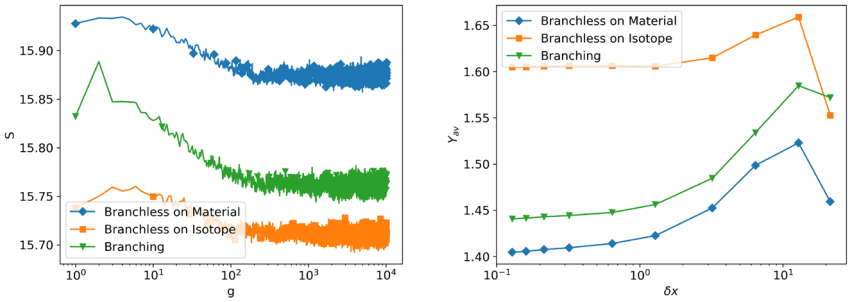

(a) Shannon entropy of the mini-core with $B = 100^3$, up to $G = 10400$ generations, and with $N = 10^5$ particles.

(b) Average Feynman moment of the mini-core, scored over 10^5 active generations with $N = 10^5$ particles.

Figure 3: Entropy and average Feynman moment for the 3D-C5G7 mini-core.

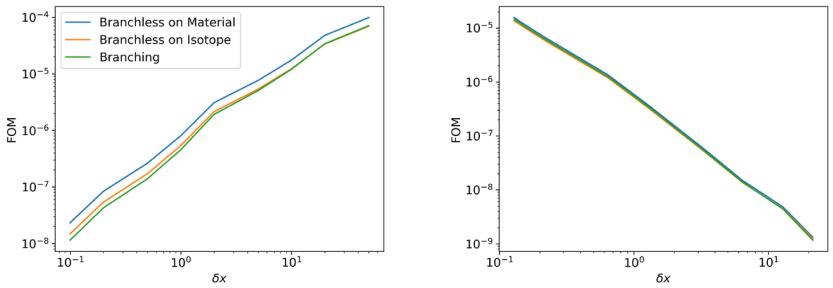

(a) Homogeneous box

(b) C5G7

Figure 4: Figure of merit defined as $FOM = 1/(\sigma_{\text{av}}^2)$ as a function of the bin size δx.

relative difference between the Feynman moments of branchless collisions on the isotope and branching collisions, with respect to branchless collisions on the material, defined by

$$R_{\text{iso/b}} = \frac{Y_{iso/b} - Y_{\text{mat}}}{Y_{\text{mat}}}, \tag{11}$$

where Y_{iso} denotes the Feynman moment when using branchless collisions on the isotope, Y_{b} denotes the Feynman moment when using branching collisions, and Y_{mat} denotes the Feynman moment when using branchless collisions on the material. It appears that $R_{\text{iso}} \sim 15\%$ on average, indicating that using branchless collisions on the isotope actually leads to a larger amount of spatial correlations in the system compared to branchless collisions on the material. On the other hand $R_{\text{b}} \sim 3\%$ on average in the MOX assemblies, and $R_{\text{b}} \sim 1.5\%$ in the UO2 assemblies, indicating that using branchless collisions on the material provides little improvement compared to the regular branching method in the bulk of the system. $R_{\text{b}} \sim 10\%$ near the leakage boundary conditions indicates that using branchless collisions on the material does more to reduce correlations near such boundaries.

The average Feynman moment as a function of δx is plotted in Fig. 3b. All algorithms have a maximum near $\delta x = 12.85$ cm. This behaviour has previously been observed in a

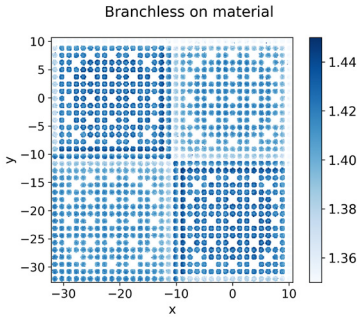

(a) Feynman moment when using branchless collisions on the material

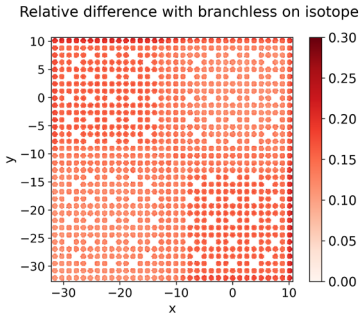

(b) Relative difference between Y_{iso} and Y_{mat}

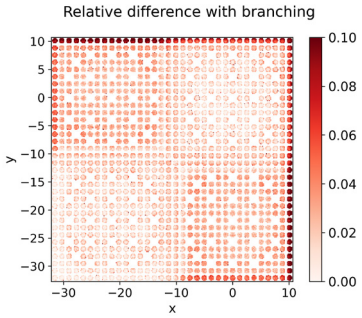

(c) Relative difference between Y_{b} and Y_{mat}

Figure 5: Feynman moments of the fission source integrated over z for $\delta x = \delta y = 0.128$ cm, scored over 10^5 active generations with $N = 10^5$ particles.

multi-group framework, and the position of the maximum was related to the typical distance over which spatial correlations develop [5]. The Feynman moment when performing branchless collisions on the material is always the smallest amongst the three collision algorithms, whereas branching collisions and branchless collisions on the isotope seem to perform similarly for coarser tallying meshes.

Lastly, we provide a short discussion regarding the figure of merit (FOM) defined as $FOM = 1/(\sigma^2_{\text{av}} T)$, where T is the total computation time and σ^2_{av} is the space-averaged (true) variance of the fission source. Fig. 4a shows that the FOM for the homogeneous box follows a positive power law with respect to δx. Using branchless collisions on the material results in a FOM that is twice as large when compared to the other methods. Fig. 4b shows that the FOM for C5G7 follows a negative power law, and close inspection shows using branchless collisions on the material yields a slightly higher FOM. This difference in behavior can be attributed to the small heterogeneous scale (i.e. the scale at which material change occurs): one can expect that the variance in a bin will be smaller if the bin size is close to the heterogeneous scale.

5 Conclusions

In this work, we presented an analysis of the spatial correlations induced by different collision algorithms in continuous energy. We recalled two variants for branchless collisions (on

the material or on the isotope), and we compare their performance with branching collisions which is customarily used in Monte Carlo transport codes. By first revisiting a continuous energy reflected critical box, we showed that for homogeneous systems with a large dominance ratio, using branchless collisions on the material helps considerably in reducing spatial correlations in the fission source. On the other hand, using branchless collisions on the isotope leads to no improvement. We extended our investigation to the 3D-C5G7 benchmark, and showed that in this case using branchless collisions on the material still resulted in some improvement, but less than in the homogeneous case. Using branchless collisions on the isotope proved to be inefficient. The last conclusion is concerning, given the fact that the branchless collisions on the isotope method is often used in a time-dependent context. Future works will focus on elucidating the conditions dictating how efficient using branchless collisions on the material is compared to regular branching collisions. The effect on different observables (such as reactions rates) and different types of estimators (e.g. collision based, track-length based...) should also be considered, as well as an extension to heterogeneous systems with much larger dominance ratios, where the advantages of using branchless collisions on the material could be more apparent.

6 Acknowledgments

This work was partially supported by the UK Engineering and Physical Sciences Research Council program grant Mathematical Theory of Radiation Transport: Nuclear Technology Frontiers (MaThRad). Grant number EP/W026899/2.

References

[1] I. Lux, L. Koblinger, *Monte Carlo particle transport methods: neutron and photon calculations* (CRC Press, Boca Raton, 1991), ISBN 978-0-8493-6074-9
[2] R. Brissenden, A. Garlick, Annals of Nuclear Energy **13**, 63 (1986)
[3] J. Miao, B. Forget, K. Smith, Annals of Nuclear Energy **92**, 81 (2016)
[4] E. Dumonteil, R. Bahran, T. Cutler, B. Dechenaux, T. Grove, J. Hutchinson, G. McKenzie, A. McSpaden, W. Monange, M. Nelson et al., Communications Physics **4**, 1 (2021)
[5] T. Bonnet, H. Belanger, D. Mancusi, A. Zoia, Nuclear Science and Engineering pp. 1–28 (2024)
[6] K. Fröhlicher, E. Dumonteil, L. Thulliez, J. Taforeau, M. Brovchenko, Nuclear Science and Engineering pp. 1–18 (2023)
[7] Belanger, Hunter, Bonnet, Théophile, Mancusi, Davide, Zoia, Andrea, *The Effect of Branchless Collisions on Neutron Clustering*, in *M&C23 International Conference on Mathematics and Computational Methods Applied to Nuclear Science and Engineering* (Niagara Falls, Ontario, Canada, 2023)
[8] Thomas E. Booth, Radiation Protection & Shielding Topical Meeting (1996)
[9] NEA, *Benchmark Calculations of Power Distribution Within Assemblies, Phase II: Comparison of Data Reduction and Power Reconstruction Methods in Production Codes* (2000)
[10] M. Nowak, J. Miao, E. Dumonteil, B. Forget, A. Onillon, K.S. Smith, A. Zoia, Annals of Nuclear Energy **94**, 856 (2016)
[11] T.M. Sutton, Nuclear Science and Engineering **185**, 174 (2017)
[12] T. Ueki, F.B. Brown, D.K. Parsons, D.E. Kornreich, Nuclear Science and Engineering **145**, 279 (2003)
[13] M. Faucher, D. Mancusi, A. Zoia, Annals of Nuclear Energy **120**, 74–88 (2018)